UMERC+OREC
2025 Conference

12-14 August | Corvallis, OR USA

Control Framework Design for WECs with Direct Drive Linear Generator-Based Power Take Off Systems

Usman Masood[a1], Mohamed A. Shabara[b], Jeff Grasberger[c], Martin Wosnik[d], Arezoo Hasankhani[a],

[a]*Department of Electrical and Computer Engineering, University of New Hampshire, Durham, NH 03824, USA*
[b]*National Renewable Energy Laboratory (NREL), Golden, CO 80401, USA*
[c]*Sandia National Laboratories, Albuquerque, NM 87123, USA*
[d]*Atlantic Marine Energy Center (AMEC), Department of Mechanical Engineering, University of New Hampshire, Durham, NH 03824, USA*

Abstract

Ocean wave energy conversion has attained significant research interest due to its vast untapped potential, offering promising solutions for powering Blue Economy (PBE) applications in remote maritime locations where traditional grid connections are impractical or cost prohibitive. However, the efficient and reliable conversion of ocean wave energy remains challenging due to the variability of ocean conditions, the complexities of energy conversion processes, and the need for robust control to ensure stable and consistent power output. The complex and nonlinear behavior of ocean waves further necessitates the use of nonlinear control strategies to maximize energy capture, reduce cost and maintain reliable system performance. This study introduces a comprehensive control framework for Wave Energy Converter (WEC) and Permanent magnet linear synchronous generator (PMLSG) based Power Take-Off (PTO) system, consisting of three main stages: wave energy capture, mechanical-to-electrical conversion, and electrical power conditioning. The focus is on the first-stage controller, designed to synchronize the WEC's motion with ocean waves to maximize energy extraction using Sliding Mode Control (SMC), benchmarked against Proportional-Integral (PI) control. Also, comparison has been performed with and without Control Force Limit (CFL). The energy absorbed using SMC was 9.7% higher than that achieved with PI control. The proposed SMC ensures robust performance under system nonlinearities and environmental uncertainties, enhancing the overall efficiency and reliability of WECs for PBE applications.

[1] ∗ Usman Masood.
E-mail address: um1023@usnh.edu

Keywords: Wave Energy Converter (WEC); Sliding Mode Control (SMC); Direct Drive Linear Generator (DDLG); Power Take Off (PTO); Blue Economy (PBE)

1 Introduction

Wave energy is emerging as a reliable and high-density renewable resource with the potential up to two terawatts of power worldwide, can play a significant role in the global energy transition [1]. Wave energy supports grid stability, reduces dependence on large-scale storage, and plays a key role in Powering the Blue Economy (PBE). Advanced control strategies are essential for maximizing energy capture, improving reliability, and enabling sustainable integration. Several control strategies have been developed for WECs, including Complex-Conjugate Control (CCC), Latching, and Model Predictive Control (MPC) [2]. In the CCC approach, optimal energy absorption is achieved by adjusting the PTO resistance and reactance to compensate for the system's inherent hydrodynamic characteristics [3]. Latching control involves constraining the motion of the device using dedicated mechanisms, which can be unreliable [4, 5]. MPC require wave prediction and is computationally demanding for real-time implementation [6]. Maximum energy conversion occurs when the device operates in phase with the excitation force [3]. This condition can be achieved through methods such as Singular Arc (SA) control [7] and multi-resonant feedback control [8]. Linear-model-based control often proves suboptimal and increases the levelized cost of energy (LCoE). SMC is recognised for its robustness and suitability for nonlinear systems, and has been extensively applied across various domains [9, 10]. Fig 1 illustrates a wave energy conversion system with a three-stage control architecture. In the first stage, the buoy captures wave energy and converts it into mechanical motion, which is transformed into electrical energy by the PTO in the second stage. The third stage conditions the irregular electrical output into a stable form suitable for grid integration and PBE applications.. There is a need of control in all three stages. The second stage of the PTO system can be broadly classified into two main categories: linear direct-drive and indirect-drive mechanisms.

In summary, a nonlinear model is essential for accurately predicting WEC behavior, particularly with nonlinear geometries. This paper presents the implementation of SMC in wave energy conversion using a nonlinear hydrodynamic body ellipsoid. The primary objective is to implement and evaluate a first-stage control that synchronizes WEC dynamics with ocean wave motion to maximize energy absorption. SMC performance is benchmarked against a conventional PI controller within a nonlinear WEC model, both with and without CFL. Stability is demonstrated through Lyapunov's analysis and validated by numerical simulations in MATLAB using WEC-Sim. Additionally, a generator model converts mechanical motion to electrical output, offering computational efficiency for early-stage design. The project is open-source and can be accessed via GitHub repository.

2 WEC and PMLSG Model

In this study, we consider a single degree of freedom (DOF) point absorber, heave dynamics are described by [11]:

$$m_r \ddot{x} = F_e + u + F_{hs} + F_r \tag{1}$$

where m_r is the mass, $\ddot{x}$ is the vertical acceleration, F_e is the wave excitation force, u is the control force, F_{hs} is the hydrostatic restoring force, and F_r is the radiation force. Formulation of the forces has been provided in appendix A.

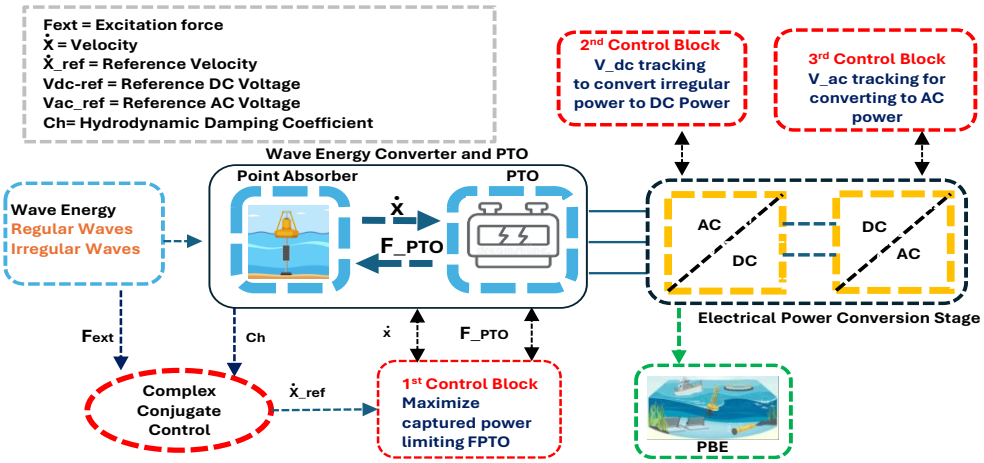

Figure 1: Framework of Wave Energy Conversion Stages and Control

The absorbed energy W over time $[0, t]$ is computed as [12]:

$$W = \int_0^t F_c \, \dot{x} \, dt \tag{2}$$

where F_c is the control force and $\dot{x}$ is the velocity. The model of PMLSG for wave energy conversion, focusing of design variables, voltage induction, and electrical dynamics has been presented from [13]. The heave and the velocity produced by WEC control simulation for regular and linear case using WEC-Sim become input to the PMLSG model to evaluate the electrical power. This model is not computationally expensive and provides insight into the electrical power output while keeping it simple by neglecting the impact of electromagnetic force. The induced phase voltage for three phase due to translator motion is given by:

$$e_{\text{ph}} = K_E \cos\left(\frac{\pi}{\tau} z\right) v(t), \tag{3}$$

Here, z is translator displacement, $v(t)$ is velocity, K_E is the back-EMF constant. In this framework, electromagnetic reaction is neglected. This model forms the basis for simulating generator behavior under simplified conditions. Details of design variables and values of the parameters used in simulation are listed in Appendix A table 1.

3 SMC Control Formulation

The SMC has been selected for regulating the nonlinear dynamics of the WEC due to its robustness against system uncertainties. The model of nonlinear WEC can be expressed as [14]:

$$\dot{x}_2 = \frac{1}{M}(F_e - F_r - F_{hs} - u) \tag{4}$$

The system's acceleration is denoted by $\dot{x}_2$. The excitation force F_e and radiation force F_r are defined in equations (14) and (16) in appendix. The control input is u. The effective mass is $M = m + m_\infty$, where m is the buoy mass and m_∞ is the added mass. The reference velocity x_{2ref} is set to align with the excitation force's frequency and phase for optimal energy capture can be defined as follows [3].

$$x_{2ref} = \frac{F_e}{2c_h}, \dot{x}_{2ref} = \frac{\dot{F}_e}{2c_h} \tag{5}$$

Here c_h is the hydrodynamic damping coefficient. After defining tracking errors, sliding surface and to ensure Lyapunov's stailty criteria control law for can be formulated as follows.

$$u = F_e - F_r - F_{hs} - m\left(\dot{x}_{2\text{ref}} - \frac{l}{a}\,\text{sign}(s)\right) \tag{6}$$

4 Results and Discussion

The system response was simulated in MATLAB using WEC-Sim to model the device and PTO unit, with the global reference frame connected to one end of the PTO and the buoy attached to the other. The controller regulated the relative motion between the reference frame and buoy using the SMC output. To capture the nonlinear dynamics, an ellipsoidal buoy with a major axis of 10 [m] and minor axis of 5 [m] was used. A fixed time step of 0.01 [s] over a total duration of 350 [s] was applied under regular waves with a wave height of 0.8222 [m] and period of 6 [s]. The hydrodynamic forces acting on the system were modeled nonlinearly, and quadratic drag was included. This section compares the performance of two control strategies with CFL $\in \left[-4 \times 10^5,\ 4 \times 10^5\right]$ N and without CFL, SMC with a signum function and a conventional Proportional-Integral (PI) controller [15]. Fig 2 shows the comparison of energy absorbed between SMC and PI with CFL and without CFL. It can be observed the CFL did not impact the energy absorbed 11.2 [MJ] in case PI and 12.4 [MJ] in case of SMC. The performance of SMC is superior in terms of energy absorbed as SMC can cater the nonlinearities of Complex wave energy system. The comparative analysis of the absorbed energy demonstrates in Fig 2, that the SMC outperforms the PI controller in terms of harvested energy. Also Better performance of SMC can be observed in Fig 3, Where SMC tracks reference velocity better than PI. Fig 4 shows the control force comparison where chattering phenomena can be observed in case of SMC due to signum function and nonlinearity and magnitude of control force is slightly higher than PI, when CFL is applied, SMC hits the CFL.

Fig 5 shows the comparison of heave motion between SMC and PI controllers. The SMC exhibits slightly higher heave than PI due to the influence of the control force. It can be observed that applying a CFL not only reduces the offset in the SMC response but also helps regulate the buoy's heave motion. Notably, potential stroke issues can be mitigated by applying an appropriate CFL. Fig 6 shows the current waveforms i_1, i_2, and i_3, demonstrating balanced three-phase

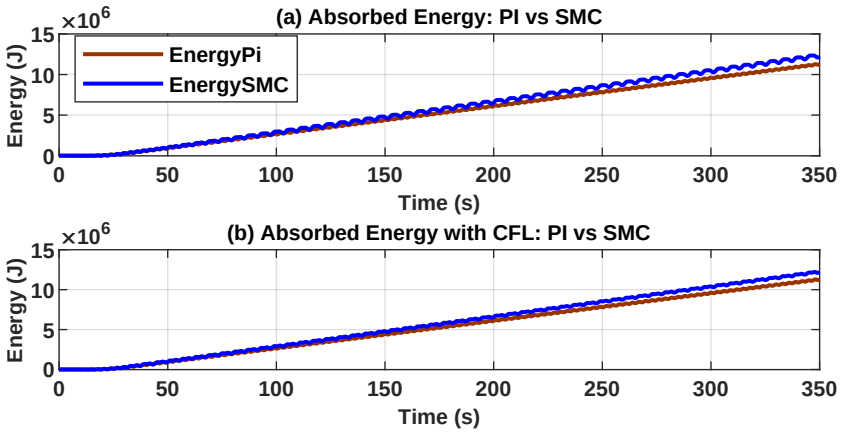

Figure 2: Comparison of Harvested Energy using PI and SMC with and without CFL

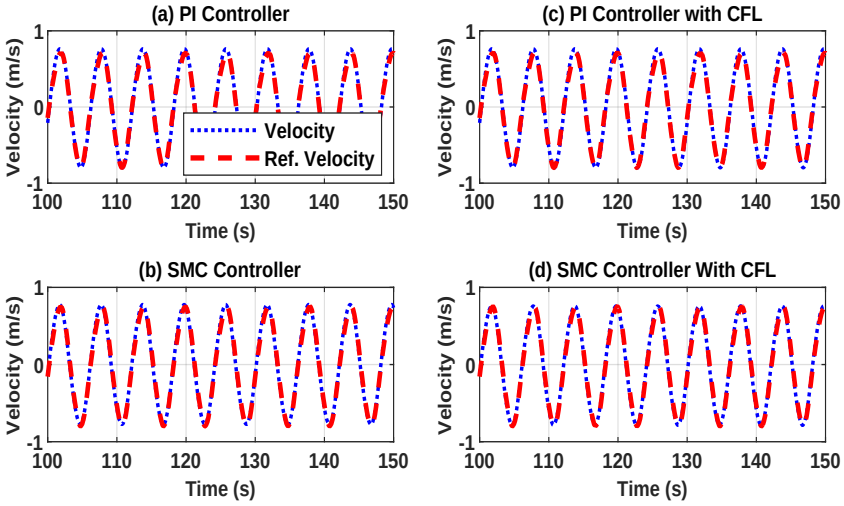

Figure 3: Comparison of Reference Velocity Tracking using PI and SMC with and without CFL

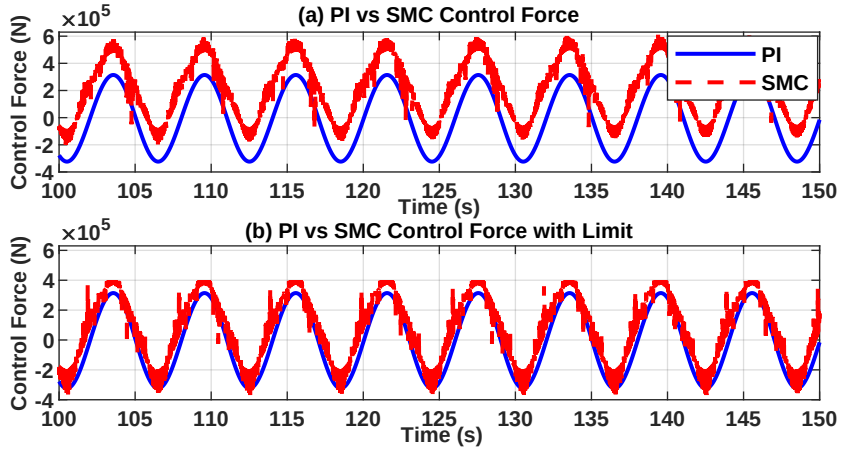

Figure 4: Comparison of Control Force Comparison using PI and SMC with and without CFL

sinusoidal behavior under regular wave excitation. The consistent amplitudes indicate stable generator operation and effective control of the phase currents. The currents are presented for one period of regular waves, illustrating the

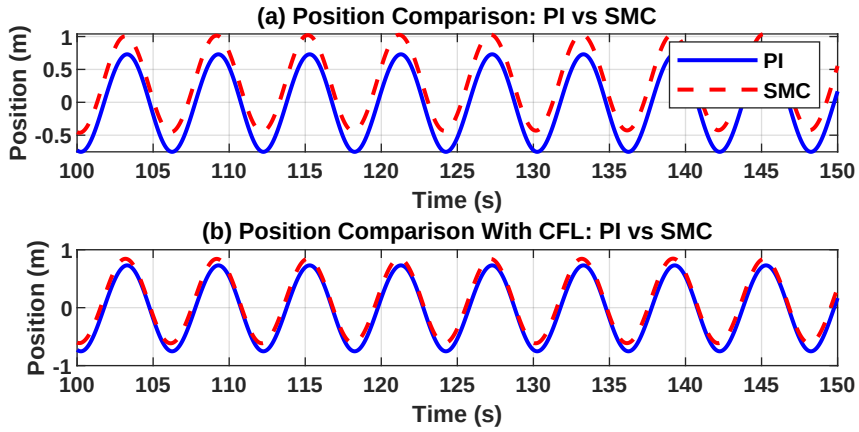

Figure 5: Comparison of Heave using PI and SMC with and without CFL

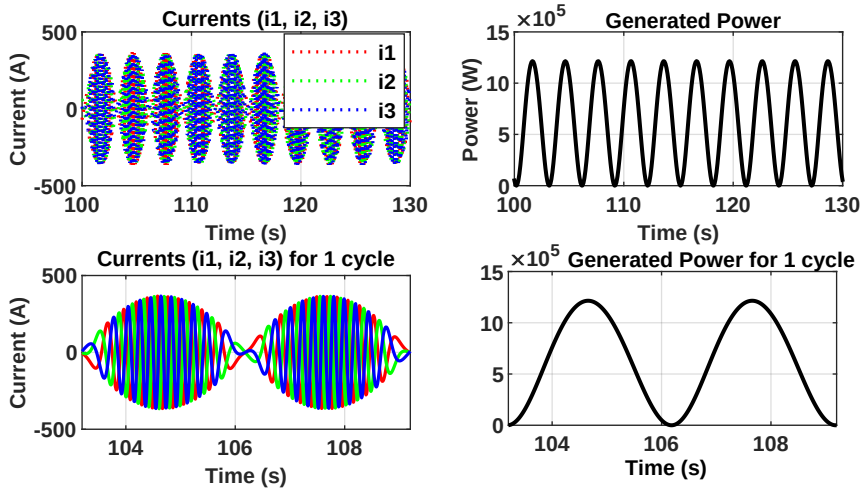

Figure 6: Generated Power from PMLSG using linear waves and linear forces

system's power output scaled to a single period under regular and linear model conditions.

Conclusion

In this study, a nonlinear wave energy conversion system was modeled and controlled using SMC and benchmarked against a conventional PI controller. The nonlinear dynamics of the WEC were simulated using WEC-Sim with an ellipsoidal buoy model, while a simplified PMLSG model was employed to estimate the electrical power output. The results demonstrate that the SMC approach offers superior performance in terms of energy absorption and reference velocity tracking. The absorbed energy with SMC reached 12.4 [MJ], which is approximately 9.7% higher than the 11.2 [MJ] achieved with PI control. The SMC also tracked the reference velocity more accurately, while the PI controller exhibited tracking errors. The application of a CFL effectively reduced the offset in heave motion for SMC, helping to mitigate potential stroke issues. The comparison of phase currents confirmed stable generator operation under both control strategies, with balanced three-phase sinusoidal waveforms observed. Overall, the proposed SMC strategy, combined with appropriate CFLs, enhances the efficiency, robustness, and safety of the WEC system, demonstrating its potential for practical deployment in PBE applications. In the Future, Electro Magnetic Force can be added to the model and SMC can be applied using real-time wave data.

Acknowledgments

The authors thank Pablo Matamala, a graduate student from the Ocean Engineering Department, for his assistance during this research.

Appendix A. An example appendix

In this study, we consider a single degree of freedom (DOF) point absorber whose heave dynamics are described by:

$$m_r \ddot{x} = F_e + u + F_{hs} + F_r \tag{7}$$

where m_r is the reference mass (including added mass), $\ddot{x}$ is the vertical acceleration, F_e is the wave excitation force, u is the control force, F_{hs} is the hydrostatic restoring force, and F_r is the radiation force.

The excitation force F_e combines the dynamic Froude–Krylov (FK) force $F_{FK_{dy}}$ and static FK component $F_{FK_{st}}$, computed from the instantaneous pressure p over the submerged surface:

$$\begin{aligned} F_{FK} &= F_{FK_{dy}} + F_{FK_{st}} = \iint_S p\vec{n}\, dS \\ &= \int_0^{2\pi} \int_{h_1}^{h_2} p f'(\sigma) f(\sigma)\, d\sigma\, d\theta \\ &= \sum_{i=1}^{N-1} \int_0^{2\pi} \int_{\sigma_i}^{\sigma_{i+1}} p f'(\sigma) f(\sigma)\, d\sigma\, d\theta \end{aligned} \tag{8}$$

Here, p is the wave-induced pressure, $\vec{n}$ is the surface normal, σ is the submerged depth, θ is the angular position, and $f(\sigma)$ defines the buoy's geometry.

The pressure p is modeled using Airy's wave theory:

$$p = \rho g \eta e^{k\sigma} \cos(\omega t - k f(\sigma) \cos\theta) - \rho g \sigma \tag{9}$$

where ρ is water density, g is gravitational acceleration, η is wave amplitude, k is wave number, ω is wave frequency, t is time, with the first term capturing dynamic pressure decay and the second term representing hydrostatic pressure.

Radiation forces are modeled as:

$$\dot{\vec{x}}_r = A_r \vec{x}_r + B_r \dot{x}, \quad F_r = -m_\infty \ddot{x} - C_r \vec{x}_r \tag{10}$$

where $\vec{x}_r$ is the radiation state vector, A_r, B_r, C_r are system matrices from hydrodynamic coefficients, $\dot{x}$ is buoy velocity, and m_∞ is the added mass at infinite frequency.

The absorbed energy W over time $[0, t]$ is computed as [12]:

$$W = \int_0^t F_c\, \dot{x}\, dt \tag{11}$$

where F_c is the control force and $\dot{x}$ is the heave velocity.

To simulate the nonlinear dynamics of the WEC, an ellipsoidal buoy geometry was modeled using WEC-Sim. The PTO unit was configured between the buoy and a fixed global reference frame. Additionally, a quadratic drag force dependent on the square of the buoy's velocity was incorporated into the model using a drag coefficient C_d and a characteristic surface area. The system was subjected to regular waves with a height of 0.8222 [m] and a period of 6 seconds.

To correct the non-uniformity caused by stator slots, Carter's coefficient K_c is used to estimate an equivalent air gap g_{eq}, improving magnetic flux calculation:

$$g_{\text{eq}} = K_c \cdot g_a, \quad K_c = \frac{\tau_t (5 g_a + b_s)}{\tau_t (5 g_a + b_s) - b_s^2} \tag{12}$$

Here, g_a is the physical air gap, τ_t is the tooth pitch, and b_s is the slot width. The equivalent air gap accounts for slotting effects, with K_c adjusting the flux path.

The phase flux density ϕ considering magnetic reluctance is:

$$\phi = \frac{B_r h_m H_c \mu_0}{h_m H_c \mu_0 - g_{\text{eq}} B_r} \tag{13}$$

where B_r is the residual flux density, h_m is magnet height, H_c is coercive force, and μ_0 is vacuum permeability.

The induced phase voltage due to translator motion is:

$$e_{\text{ph}} = K_E \cos\left(\frac{\pi}{\tau} z\right) v(t), \quad K_E = M_s W_s N_{\text{ph}} \phi v_{\text{av}}, \quad v_{\text{av}} = \frac{2}{\pi} v_m \tag{14}$$

Here, z is translator displacement, $v(t)$ is velocity, K_E is the back-EMF constant, M_s and W_s are magnet and slot dimensions, N_{ph} is number of turns per phase, and v_m is peak velocity.

The three-phase voltages are:

$$e_1 = K_E \cos\left(\frac{\pi}{\tau} z\right) v(t), \quad e_2 = K_E \cos\left(\frac{\pi}{\tau} z - \frac{2\pi}{3}\right) v(t), \tag{15}$$

$$e_3 = K_E \cos\left(\frac{\pi}{\tau} z - \frac{4\pi}{3}\right) v(t) \tag{16}$$

representing balanced sinusoidal voltages in a three-phase system.
For a resistive load R_L, the terminal voltage of each phase is:

$$v_j = i_j R_L, \quad j = 1, 2, 3 \tag{17}$$

where i_j and v_j are current and voltage of phase j.
Assuming no electromagnetic feedback on the translator (simple model), the electrical dynamics are:

$$\frac{di_1}{dt} = \frac{e_1 - v_1 - i_1 R_a}{L_s}, \quad \frac{di_2}{dt} = \frac{e_2 - v_2 - i_2 R_a}{L_s}, \quad \frac{di_3}{dt} = \frac{e_3 - v_3 - i_3 R_a}{L_s} \tag{18}$$

where R_a and L_s are phase resistance and inductance, respectively. In this simplified framework, buoy velocity is driven by wave excitation $u(t)$, and electromagnetic reaction is neglected. This model forms the basis for simulating generator behavior under simplified conditions.

Parameter Description	**Notation**	**Specified Value**	**Unit**
Total number of electrical phases	m	3	–
Total magnetic poles	p	6	–
Slot count per pole per phase	q	1	–
Active armature segments	M_s	4	–
Coil windings per turn	N	82	–
Axial length of stator	L	0.432	m
Width of stator segment	W_s	0.2	m
Nominal air gap spacing	g_a	0.002	m
Magnet thickness	h_m	0.006	m
Maximum flux density in translator	B_r	1.2	T
Coercivity of magnetic material	H_c	905000	A/m
Internal resistance of armature coil	R_a	1.5	Ω
Resistive load connected per phase	R_L	7.5	Ω
Per-phase synchronous inductance	L_s	0.115	H

Table 1: Electrical and geometric specifications of the generator used in modeling.

Authors including an appendix section should do so before References section. Multiple appendices should all have headings in the style used above. They will automatically be ordered A, B, C etc.

References

[1] K. Gunn and C. Stock-Williams. “Quantifying the potential global market for wave power”. In: *Proceedings of the 4th International Conference on Ocean Engineering (ICOE 2012)*. Available online: https://www.icoe-conference.com/publication/quantifying_the_potential_global_market_for_wave_power/ (accessed on 25 August 2021). Dublin, Ireland, Oct. 2012, pp. 1–7.

[2] A. Maria-Arenas et al. “Control Strategies Applied to Wave Energy Converters: State of the Art”. In: *Energies* 12.16 (2019), p. 3115. DOI: 10.3390/en12163115.

[3] J. Falnes and A. Kurniawan. *Ocean Waves and Oscillating Systems: Linear Interactions Including Wave-Energy Extraction*. Cambridge, UK: Cambridge University Press, 2020. ISBN: 978-1-108-48166-3.

[4] A. Babarit and A.H. Clément. "Optimal latching control of a wave energy device in regular and irregular waves". In: *Applied Ocean Research* 28 (2006), pp. 77–91. DOI: 10.1016/j.apor.2006.02.003.

[5] J. Todalsphaug, T. Bjarte-Larsson, and J. Falnes. "Optimum Reactive Control and Control by Latching of a Wave-Absorbing Semisubmerged Heaving Sphere". In: *Proceedings of the International Conference on Offshore Mechanics and Arctic Engineering (OMAE)*. Vol. 4. Oslo, Norway, 2002, pp. 415–423.

[6] J. Cretel et al. "An Application of Model Predictive Control to a Wave Energy Point Absorber". In: *IFAC Proceedings Volumes* 43 (2010), pp. 267–272. DOI: 10.3182/20100712-3-DE-2013.00177.

[7] Shangyan Zou et al. "Optimal control of wave energy converters". In: *Renewable Energy* 103 (2017), pp. 217–225. ISSN: 0960-1481. DOI: https://doi.org/10.1016/j.renene.2016.11.036. URL: https://www.sciencedirect.com/science/article/pii/S0960148116310059.

[8] O. Abdelkhalik et al. "Multiresonant feedback control of a three-degree-of-freedom wave energy converter". In: *IEEE Transactions on Sustainable Energy* 8.4 (2017), pp. 1518–1527. DOI: 10.1109/TSTE.2017.2705714.

[9] Usman Masood et al. "Robust adaptive nonlinear control of plugin hybrid electric vehicles for vehicle to grid and grid to vehicle power flow with hybrid energy storage system". In: *ISA transactions* 139 (2023), pp. 406–424.

[10] Mubariz Ahmed et al. "Barrier function based adaptive sliding mode controller for the hybrid energy storage system of plugin hybrid electric vehicles". In: *Journal of Energy Storage* 72 (2023), p. 108051.

[11] Shangyan Zou, Jiajun Song, and Ossama Abdelkhalik. "A sliding mode control for wave energy converters in presence of unknown noise and nonlinearities". In: *Renewable Energy* 202 (2023), pp. 432–441.

[12] J. Falnes. "A review of wave-energy extraction". In: *Marine Structures* 20.4 (2007), pp. 185–201.

[13] Xin Niu. "Modeling and design analysis of a permanent magnet linear synchronous generator". In: (2013).

[14] Shangyan Zou et al. "Optimal control of wave energy converters". In: *Renewable energy* 103 (2017), pp. 217–225.

[15] WEC-Sim Team. *WEC-Sim Advanced Features Documentation*. https://wec-sim.github.io/WEC-Sim/dev/user/advanced_features.html#id33. Accessed: June 22, 2025. 2023.